Spatial characterisation of β-catenin-mutated hepatocellular adenoma subtypes by proteomic profiling of the tumour rim

Authors

Sylvaine Di Tommaso, Cyril Dourthe, Jean-William Dupuy, Nathalie Dugot-Senant, David Cappellen, Hélène Cazier, Valérie Paradis, Jean-Frédéric Blanc, Brigitte Le Bail, Charles Balabaud, Paulette Bioulac-Sage, Frédéric Saltel, Anne-Aurélie Raymond

Correspondence

anne-aurelie.raymond@inserm.fr (A.-A. Raymond), frederic.saltel@inserm.fr (F. Saltel).

Graphical abstract

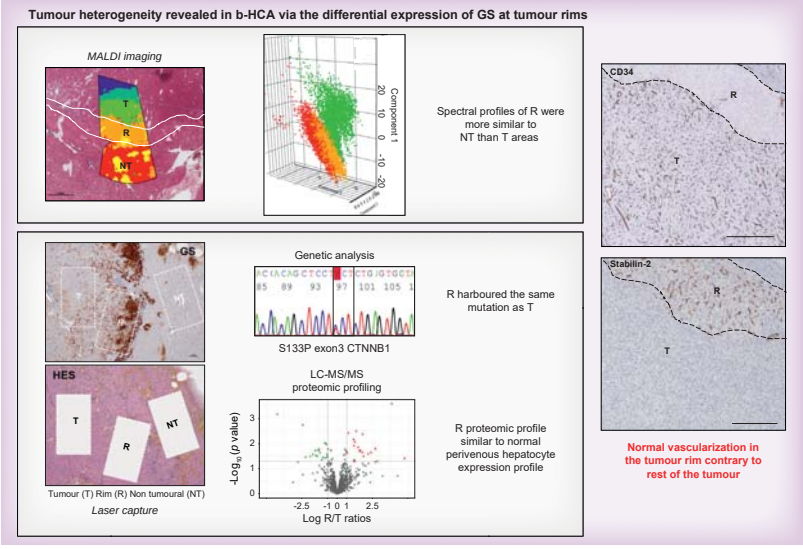

Highlights

- Tumour heterogeneity was revealed in β-catenin-mutated hepatocellular adenomas.
- The combination of several spatial approaches (MALDI imaging, genetic, and proteomic analyses) enabled us to characterise it.
- The tumour rim harboured the same mutation as the tumour centre, meaning both parts belong to the same tumour.
- However, the profiles of the tumour rim are closer to those of the non-tumoural liver than to those of the rest of the tumour.
- Normal peripheral venous drainage, demonstrated by the expression of stabilin-2 only in the tumour rim, could explain this phenotype.

Impact and implications

Tumour heterogeneity was revealed in β-catenin-mutated hepatocellular adenomas (b-HCAs) via the differential expression of glutamine synthase at tumour rims. The combination of several spatial approaches (mass spectrometry imaging, genetic, and proteomic analyses) after laser capture microdissection allowed identification of a potential role for peripheral venous drainage underlying this difference. Through this study, we were able to illustrate that beyond a mutational context, many factors can downstream regulate gene expression and contribute to different clinicopathological phenotypes. We believe that the combinations of spatial analyses that we used could be inspiring for all researchers wanting to access heterogeneity information of liver tumours.

https://doi.org/10.1016/j.jhepr.2023.100913

Research article

JHEP|Reports

Spatial characterisation of β-catenin-mutated hepatocellular adenoma subtypes by proteomic profiling of the tumour rim

Sylvaine Di Tommaso,[1,2,†] **Cyril Dourthe**,[1,2,†] Jean-William Dupuy,[3] Nathalie Dugot-Senant,[4] David Cappellen,[1,5] Hélène Cazier,[6] Valérie Paradis,[6] Jean-Frédéric Blanc,[1,7] Brigitte Le Bail,[1,8] Charles Balabaud,[1] Paulette Bioulac-Sage,[1] Frédéric Saltel,[1,2,‡,*] Anne-Aurélie Raymond[1,2,‡,*]

[1]*Université Bordeaux, Inserm UMR1312 BoRdeaux Institute of onCology (BRIC), Bordeaux, France;* [2]*Oncoprot Platform, TBM-Core US 005, Bordeaux, France;* [3]*Université Bordeaux, Proteomics Platform, Bordeaux, France;* [4]*Histology Platform, TBM-Core US 005, Bordeaux, France;* [5]*Bordeaux University Hospital Center, Tumor Bank and Tumor Biology Laboratory, Pessac, France;* [6]*Pathology Department, Henri Mondor AP-HP Hospital, Créteil, France;* [7]*Department of Hepatology and Oncology, Bordeaux University Hospital, INSERM CIC 1401, Bordeaux, France;* [8]*Pathology Department, Bordeaux University Hospital, Bordeaux, France*

JHEP Reports **2024.** https://doi.org/10.1016/j.jhepr.2023.100913

Background & Aims: Hepatocellular adenomas (HCAs) are rare, benign, liver tumours classified at the clinicopathological, genetic, and proteomic levels. The β-catenin-activated (b-HCA) subtypes harbour several mutation types in the β-catenin gene (*CTNNB1*) associated with different risks of malignant transformation or bleeding. Glutamine synthetase is a surrogate marker of β-catenin pathway activation associated with the risk of malignant transformation. Recently, we revealed an overexpression of glutamine synthetase in the rims of exon 3 S45-mutated b-HCA and exon 7/8-mutated b-HCA compared with the rest of the tumour. A difference in vascularisation was found in this rim shown by diffuse CD34 staining only at the tumour centre. Here, we aimed to characterise this tumour heterogeneity to better understand its physiopathological involvement.

Methods: Using mass spectrometry imaging, genetic, and proteomic analyses combined with laser capture microdissection, we compared the tumour centre with the tumour rim and with adjacent non-tumoural tissue.

Results: The tumour rim harboured the same mutation as the tumour centre, meaning both parts belong to the same tumour. Mass spectrometry imaging showed different spectral profiles between the rim and the tumour centre. Proteomic profiling revealed the significant differential expression of 40 proteins at the rim compared with the tumour centre. The majority of these proteins were associated with metabolism, with an expression profile comparable with a normal perivenous hepatocyte expression profile.

Conclusions: The difference in phenotype between the tumour centres and tumour rims of exon 3 S45-mutated b-HCA and exon 7/8-mutated b-HCA does not depend on *CTNNB1* mutational status. In a context of sinusoidal arterial pathology, tumour heterogeneity at the rim harbours perivenous characteristics and could be caused by a functional peripheral venous drainage.

Impact and implications: Tumour heterogeneity was revealed in β-catenin-mutated hepatocellular adenomas (b-HCAs) via the differential expression of glutamine synthase at tumour rims. The combination of several spatial approaches (mass spectrometry imaging, genetic, and proteomic analyses) after laser capture microdissection allowed identification of a potential role for peripheral venous drainage underlying this difference. Through this study, we were able to illustrate that beyond a mutational context, many factors can downstream regulate gene expression and contribute to different clinicopathological phenotypes. We believe that the combinations of spatial analyses that we used could be inspiring for all researchers wanting to access heterogeneity information of liver tumours.

© 2023 The Authors. Published by Elsevier B.V. on behalf of European Association for the Study of the Liver (EASL). This is an open access article under the CC BY-NC-ND license (http://creativecommons.org/licenses/by-nc-nd/4.0/).

Introduction

Hepatocellular adenomas (HCAs) are rare, benign, liver tumours that develop mainly in women taking long-term oral contraception.[1,2] The two main risks of HCA are bleeding[3,4] and malignant transformation into hepatocellular carcinoma (HCC),[5] with both risks related to tumour size and molecular subtype. HCAs have been classified into four subtypes according to their mutations and clinicopathological features[5–9]: (1) H-HCA, with inactivating mutations of *HNF1A*[7]; (2) inflammatory HCA (IHCA), exhibiting various mutations (interleukin 6 cytokine family signal transducer, fyn-related kinase, signal transducer and activator of transcription 3, janus kinase 1, and G-protein alpha-subunit) or chromosome

Keywords: Hepatocellular adenoma; Tumour heterogeneity; Tumour rim; β-Catenin mutation; Glutamine synthetase; Proteomic profiling.

Received 20 February 2023; received in revised form 6 September 2023; accepted 9 September 2023; available online 22 September 2023

† These authors have contributed equally.

‡ These authors share last authorship.

* Corresponding authors. Address: Inserm UMR1312 BoRdeaux Institute of onCology (BRIC), 146 rue Leo Saignat, 33076 Bordeaux, France. Tel.: +33-(0)5-57-57-95-81 (A.-A. Raymond); +33-(0)5-57-57-17-07 (F. Saltel).

E-mail addresses: anne-aurelie.raymond@inserm.fr (A.-A. Raymond), frederic.saltel@inserm.fr (F. Saltel).

alterations that activate the JAK/STAT signalling pathway[6,10]; (3) β-catenin-mutated HCA (b-HCA), with mutations in the *CTNNB1* gene encoding β-catenin[7,11] (these have the highest malignant transformation rate[12]); and (4) sonic-hedgehog-HCA, defined by microdeletions fusing the inhibin subunit beta E promotor with the *GLI* gene (these have a high haemorrhage risk).[6,13,14]

Resection is generally recommended when the HCA reaches 5 cm, except for b-HCA. Resection is systematic for b-HCA if the β-catenin pathway is activated, regardless of size, owing to the risk of malignant transformation.[15] B-HCA represents 10–15% of patients with HCA and may coexist in 10% of IHCA (b-IHCA).[6] The *GLUL* gene, a β-catenin target gene encoding glutamine synthetase (GS), is known to be specifically expressed in perivenous hepatocytes in proximity of the central vein in the normal liver. GS is essential for the maintenance of low, non-toxic ammonia levels in the organism. GS is also used in routine clinical practice as an immunomarker to identify the activation of the β-catenin pathway.[7,16] A strong and diffuse expression of GS by immunohistochemistry (IHC), with or without aberrant cytoplasmic and nuclear expression of β-catenin, is the hallmark for identification of exon 3-mutated b-HCA (but not b-HCA mutated at serine S45). Exon 3-mutated b-HCA has the greatest risk of transformation into HCC.[17] However, we have previously shown by proteomic profiling that other *CTNNB1* targets are minimally activated or not at all (such as ornithine aminotransferase) in exon 3 non-S45-mutated b-HCA. Thus, the risk of malignant transformation cannot not be exclusively dependent on the activation of the β-catenin pathway.[9]

Other types of β-catenin mutations have been identified by molecular analysis: in exon 3 at S45 or exon 7/8. B–HCAs harbouring these mutations have lower levels of β-catenin pathway activation as suggested by lower levels of immunodetected GS. The exon 7/8-mutated b-HCA subtype has a very low risk of transformation into HCC, but has a significant risk of bleeding.[6,17,18] Interestingly, our previous immunohistological analysis of exon 3 S45-mutated b-HCA and exon 7/8-mutated b-HCA revealed an overexpression of GS, but with different patterns in the tumour rim (R) compared with the rest of the tumour; the rest of the tumour actually showed low GS expression.[16] A difference in vascularisation had been associated with GS-positive Rs, highlighted by diffuse CD34 staining found only at the centre of the tumour (T) in exon 3 S45-mutated HCA and exon 7/8-mutated HCA, but not in exon 3 non-S45-mutated HCA.[16] First, this finding reveals tumour heterogeneity among exon 3 S45-mutated b-HCA and exon7/8-mutated b-HCA in terms of tissue architecture (via different vascularisation) and at the protein expression level (at least differential expression of GS). Second, given that exon 3 S45-mutated b-HCA and exon 7/8-mutated b-HCA have a low risk of malignant transformation but rather a high risk of bleeding,[6,17,18] the question arises as to what drives this difference in GS expression at the R and whether it would have an effect on tumour pathophysiology.

Using innovative mass spectrometry imaging (MSI) and liquid chromatography–tandem mass spectrometry (LC-MS/MS)-based proteomic profiling, we defined the characteristics of b-HCA Rs and identified differentially expressed proteins. Our goal was to better understand what could explain the tumour heterogeneity in these b-HCA subtypes.

Materials and methods

Patients

Twenty-nine cases were selected from our b-HCA patient cohort: nine cases harboured exon 3 non-S45-mutated b-HCA, nine cases harboured exon 3 S45-mutated b-HCA, and 11 cases harboured exon 7/8-mutated b-HCA. Their clinical and pathological features have been previously described in Sempoux *et al.*[16] This HCA collection is accredited by the Cancer Biobank of Bordeaux University Hospital Center (BRIF: BB-0033-00036).

Mass spectrometry imaging

Analysis of b-HCA was performed on tissue sections (3 μm thick) mounted on indium tin oxide-coated conductive slides for matrix-assisted laser desorption/ionisation (MALDI) mass spectrometry (MS) analysis or on regular slides for H&E staining for histological analysis. All sections were dried at 37 °C overnight before analysis. For MSI analysis, sections were preheated at 85 °C for 15 min and then dewaxed with xylene (2 × 5 min). Sections were rehydrated in a series of washes for 5 min with isopropanol (100%) and ethanol (100, 96, 70, and 50%). Antigen retrieval was performed using a heat-induced epitope retrieval machine (Decloaking Chamber, BioCare Medical, Concord, CA, USA) by heating the section in H_2O at 110 °C for 20 min. Trypsin (25 μg/ml in 20 mM ammonium bicarbonate and 0.01% glycerol) was applied to tissue sections using an automatic sprayer (16 cycles at 15 μl/min, TM Sprayer, HTX Technologies). Digestion was for 3 h at 50 °C in a humid chamber with K_2SO_4 solution. An α-cyano-4-hydroxycinnamic acid MALDI matrix (10 mg/ml in acetonitrile/H_2O 70/30 v/v, 1% trifluoroacetic acid) was also applied to sections using the automatic sprayer (four cycles at 120 μl/min). MALDI MSI analysis was performed on an Autoflex III MALDI–tandem time-of-flight (TOF/TOF) mass spectrometer with a Smartbeam laser using FlexControl 3.4 and FlexImaging 4.1 software packages (Bruker Daltonics) in the range of m/z 600–3,200 at a spatial resolution of 100 μm. A standard peptide calibration mix (Bruker Daltonik GmbH) was used for external calibration. After MSI analysis, the matrix was removed from each slide by washing in 100% ethanol for 5 min. Tissue sections were then stained with H&E and examined by a pathologist to correlate MALDI MSI data with histological features in the same section. Data analysis of MALDI MSI data was performed using the SCiLS Lab Pro 2023a software (SCiLS GmbH, Bremen, Germany) from regions of interest (ROIs) corresponding to the different morphological patterns of HCA. The raw images were loaded in the SCiLS Lab software. Baseline subtraction was performed using the convolution algorithm as well as denoising. The spectra were normalised by total ion count.

Sample preparation for proteomic analysis

Fixation reversal and protein extraction from tissue sections, in-gel trypsin digestion, peptide extraction from gel, and peptide sample preparation for LC-MS/MS analysis were performed as previously described.[13]

MS analysis

Online nanoLC-MS/MS analysis was performed using an Ultimate 3000 RSLC Nano-UPHLC system (Thermo Scientific, USA) coupled to a nanospray Orbitrap Fusion™ Lumos™ Tribrid™ Mass Spectrometer. LC-MS/MS parameters have been previously described.[13,14]

Database searching, processing, and quantification of MS results

We used the Mascot 2.4 algorithm available in the Proteome Discoverer 2.5 software (Thermo Fisher Scientific) for protein identification. We used the algorithm in batch mode by

searching against the UniProt *Homo sapiens* database (73,946 entries, Reference Proteome Set, release date: 17 November 2018) from the UniProt website (http://www.uniprot.org/). Two missed cleavage sites for the trypsin were tolerated. Mass tolerances in MS and MS/MS were set to 10 ppm and 0.02 Da, respectively. Oxidation of methionine and acetylation of lysine were investigated for dynamic modifications. Carbamidomethylation of cysteine was investigated for fixed modification. Raw LC-MS/MS data were imported in Proline web[19] for feature detection, alignment, and quantification. Protein identification was only accepted after identification of at least two specific peptides with a pretty rank = 1 and with a protein false discovery rate value below 1.0% (calculated using the 'decoy' option in Mascot). Label-free quantification of MS1 level by extracted ion chromatograms was carried out using the parameters previously described.[13] Protein abundances were normalised using the 'median ratio' option in Proline Studio 2.1. The MS proteomic data were deposited in the ProteomeXchange Consortium[20] via the PRIDE partner repository with the dataset identifier PXD031323.

Bioinformatic/biostatistical analyses

Differential protein expression between T, R, and non-tumoural (NT) tissue samples from each patient was analysed by computing log ratios for the median of normalised protein abundances for each paired T/NT sample. The proteins deregulated in the R relative to the T were compared between patients to isolate the most significant variations. For this, we applied a Wilcoxon–Mann–Whitney *t* test (data without homogeneity of variance and that do not follow a normal distribution; small sample size, but sufficient for a non-parametric test). We set the significance threshold (*p* value) to 0.05. This identified a set of 40 differentially expressed proteins between the R and the T. Using this relevant dataset, we performed principal component analysis (PCA) using FactoMineR and Factoextra available in the R software (version 4.3.1). We then performed gene set enrichment analysis against the Reactome database to find pathways significantly deregulated between the T and the R.

Details of the techniques used for IHC analysis, tissue-based cell counting, laser capture, and sanger sequencing are available in the Supplementary information.

Results

The R has a different GS expression pattern but the same *CTNNB1* mutation

We combined several approaches to characterise the R of b-HCA. All analyses were performed on formalin-fixed, paraffin-embedded (FFPE) b-HCA resections (Fig. 1B). Detection of GS by IHC was used as a reference for defining the different ROIs: T, R, and adjacent NT tissues (Fig. 1A). MSI associated with histological analyses allowed us to define the main tissue features (difference between ROIs in cell content, molecular content, proliferation, or death) (Fig. 1B). We then used laser capture microdissection to isolate ROIs from the T, R, and NT areas. We performed either genetic analysis or LC-MS/MS proteomic profiling of these different isolated ROIs (Fig. 1B) to make comparisons and therefore better understand their differences (Fig. 1B).

We analysed four exon 3 S45-mutated b-HCA cases and three exon 7/8-mutated b-HCA cases, which we compared with four exon 3 non-S45-mutated b-HCA cases. We could not visualise Rs among any exon 3 non-S45-mutated b-HCA samples. For these samples, which thus served as a control, we defined the tumoural tissue front as where the NT tissue began. This border then served for isolation of outer edge (OE) tissues for exon 3 non-S45-mutated cases. We searched for β-catenin mutations in the R tissues by Sanger sequencing. We found the same *CTNNB1* gene mutation in the R tissues as the previously identified mutations in the corresponding T tissues, demonstrating thus that the R was indeed part of the same tumour (Fig. 1C).

We checked the expression levels of GS by LC-MS/MS by comparing its relative abundance between ROIs (Fig. 1D and E). In correlation with IHC results and as expected, GS was strongly expressed in T tissues compared with NT tissues from exon 3 non-S45-mutated b-HCA (average T/NT ratio = 69.57). In contrast, in exon 3 S45-mutated b-HCA, GS was downregulated in T tissues compared to NT tissues in one case (T/NT ratio = 0.55) and slightly upregulated in three cases (average of T/NT ratios = 1.84). In exon 7/8-mutated b-HCA, GS was downregulated in all the three tumours compared with corresponding NT tissues (average of T/NT ratios = 0.27) (Fig. 1D). GS expression was either unchanged or slightly downregulated (average of OE/T ratios = 0.85) in the OE in comparison with T tissues in exon 3 non-S45-mutated b-HCA (Fig. 1E). We confirmed and quantified the overexpression of GS in all R tissues of exon 3 S45-mutated and exon 7/8-mutated b-HCA (average of R/T ratios = 6.87 in exon 3 S45-mutated b-HCA and average of R/T ratios = 22.66 in exon 7/8-mutated b-HCA) (Fig. 1E).

The R is neither proliferative nor transformative

GS expression is used as a surrogate biomarker for the activation of the β-catenin pathway in contexts of malignant transformation. Even if exon 3 S45-mutated b-HCA and exon7/8-mutated b-HCA have a very low risk of progression to HCC, we still wanted to verify whether this GS-positive R was caused by an increase in tumour size or by carcinogenesis.

To test the hypothesis of progression/proliferation fronts in the R, we analysed the phosphorylation of histone H3 expression by IHC. We observed only a few phosphorylated histone H3 hepatocytes at the R of exon 3-mutated b-HCA and exon 7/8-mutated b-HCA tumours compared to the rest of the tumour (Fig. 2A). Analysis of exon 3 non-S45-mutated b-HCA did not reveal any further proliferation in the tumour periphery (Fig. 2B). Proliferation fronts can induce stress on normal adjacent tissue and induce cell death. We thus performed anti-active caspase 3 IHC, which showed no difference between normal and tumoural hepatocytes in any of the b-HCA subtypes (Fig. 2A and B). Proliferative fronts can also induce an increase in tumour cell numbers and thus an increase in cell density with compaction.[21] In this light, we measured tumour cell density in the R area. We found no difference in tumour cell numbers between the T and R for three cases (one exon 3 S45-mutated and two exon 7/8-mutated b-HCA) (Fig. S1A) or between the T and OE of three cases of exon 3 non S45-mutated b-HCA (Fig. S1B).

In a previous study, we developed a method for defining the characteristic proteomic profile of given groups of patients with HCA for diagnostic and prognostic use.[9] Briefly, we defined a signature for the malignant transformation of HCA by comparing transformed and non-transformed areas of tissue from the same tumours. Hence, here we compared the proteomic profiles of the Rs from exon 3 non-S45-mutated b-HCA and exon7/8-mutated b-HCA (calculated from R/NT ratios) with the previously determined HCA malignancy signature.[9] Using random forest testing, the

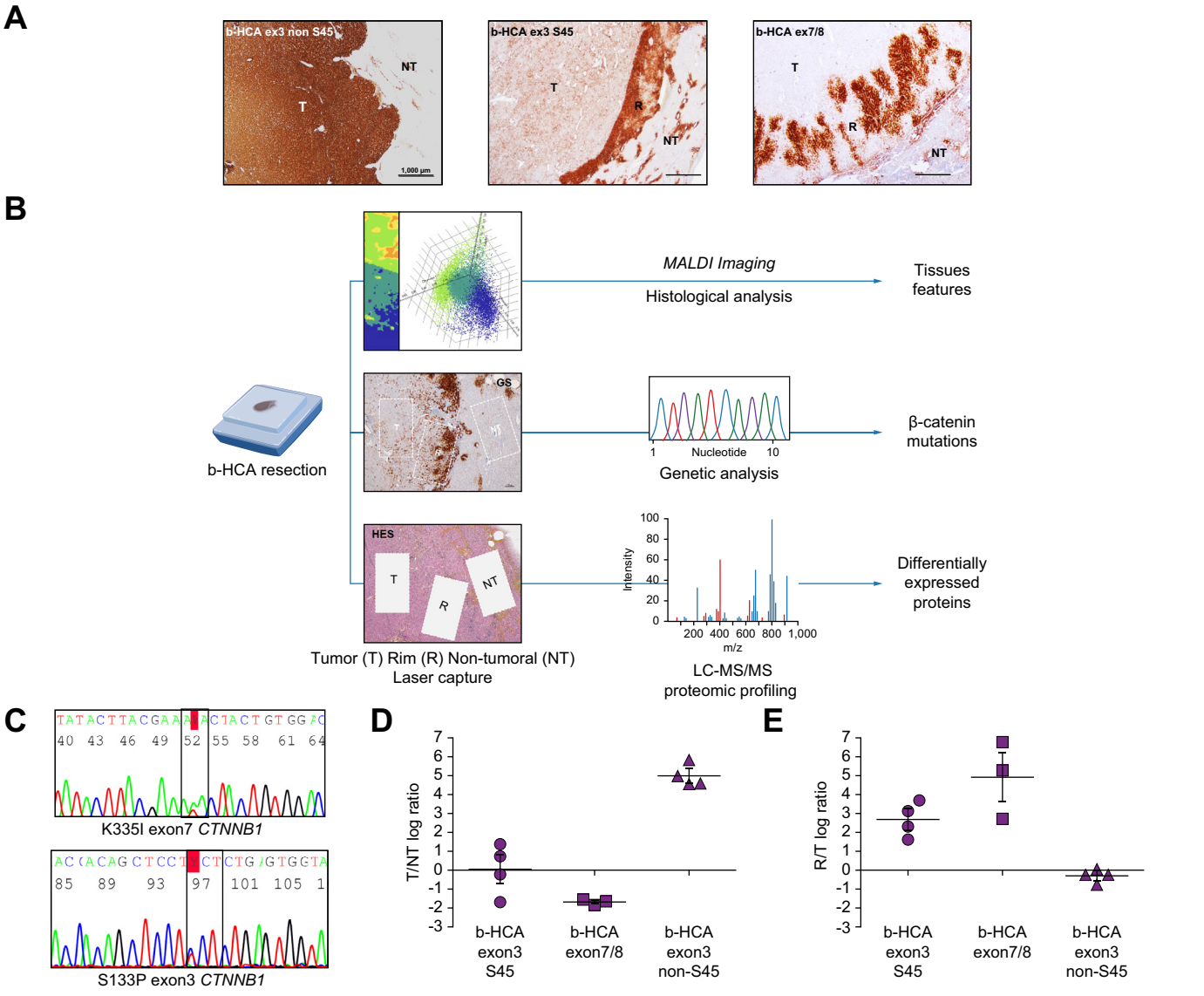

Fig. 1. Analytical strategy and different GS expression patterns. (A) GS expression patterns in the different β-catenin-mutated b-HCA subtypes (exon 3 non-S45-mutated, exon 3 S45-mutated, exon 7/8-mutated) detected by immunohistochemistry (T, R, and NT tissue). (B) Workflow of the different technological approaches used in this study to characterise the b-HCA tumour rim (MALDI imaging and laser capture microdissection of tissue areas of interest coupled with genetic or proteomic analysis). All analyses were performed on FFPE b-HCA resections. (C) Example of *CTNNB1* gene sequencing results from the R of an exon 7/8-mutated b-HCA (top) and an exon 3 S45-mutated b-HCA (bottom). The mutation is highlighted in red, and the reading frame is boxed in black. (D and E) Mass spectrometric quantification of GS expression levels in the T, R, and adjacent NT tissue: T/NT ratios (top) and R/T ratios (bottom). Fig. 1B was created with BioRender. b-HCA, β-catenin-activated HCA; FFPE, formalin-fixed, paraffin-embedded; GS, glutamine synthetase; HCA, hepatocellular adenoma; HES, H&E saffron; LC-MS/MS, liquid chromatography–tandem mass spectrometry; MALDI, matrix-assisted laser desorption/ionisation; NT, non-tumoural; R, tumour rim; T, tumour centre.

proteomic profile of the R was recognised as a non-malignant b-HCA (Fig. 2C). Similarly, the Euclidean distance was shorter between the R profile and the b-HCA subgroup profile compared with the profiles of other HCA subtypes (Euclidean distance with b-HCA = 19.07 *vs*. with other HCAs = 23.43) (Fig. 2C). The Euclidean distance was also shorter between the R profile and the profiles of other non-transformed HCAs compared with HCAs having transformed to HCC (Euclidean distance with non-transformed HCA = 3.09 *vs*. with HCC developed on HCA = 5.54) (Fig. 2C).

Overall, these results show that the overexpression of GS in the Rs of exon 3 S45-mutated b-HCA and exon 7/8-mutated b-HCA is not related to proliferation or carcinogenesis often associated with β-catenin pathway activation.

The proteomic profile of the R is similar to a normal perivenous hepatocyte expression profile

We moved on to the use of exploratory spatial approaches to understand the functional characteristics in the R. We first used MSI to explore the molecular content of these tissue areas (Fig. 3). Acquisitions were performed on T, R, and NT areas after selection by pathologists (PBS and VP) among three cases of exon 3 S45-mutated b-HCA and two cases of exon 7/8-mutated b-HCA. After MSI data processing, segmentation of these specific areas

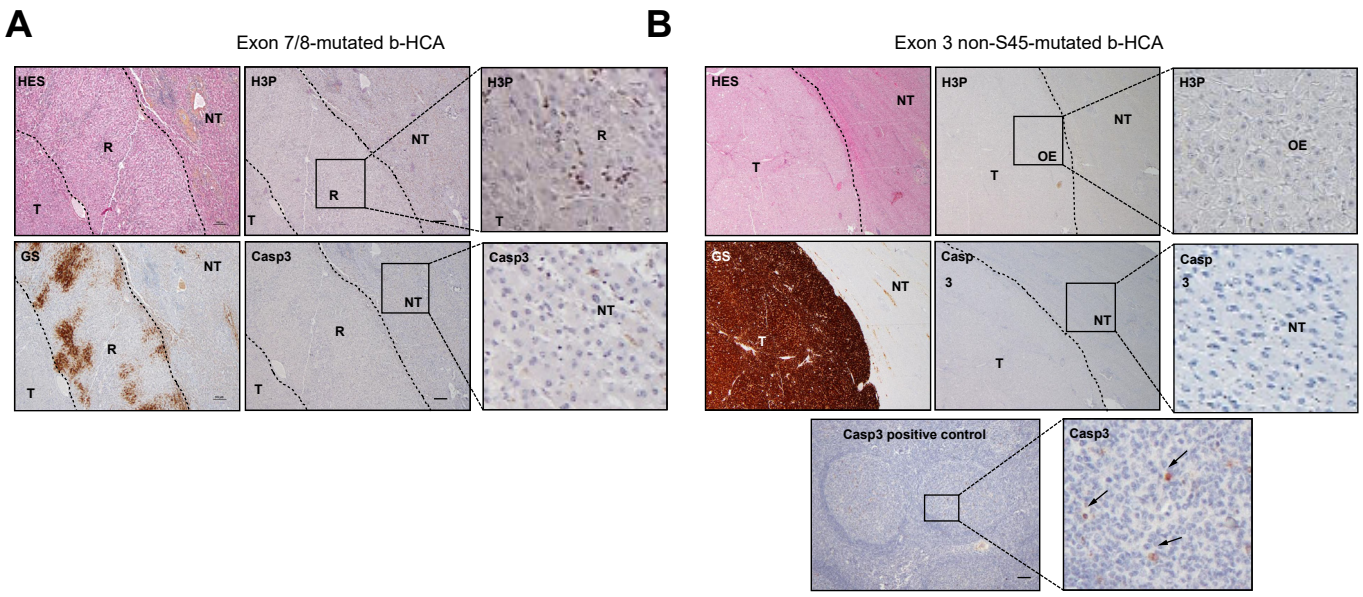

Fig. 2. Representative images of R proliferation status (anti-pHistone3) in exon 7/8-mutated b-HCA or the OE of exon 3 non 45 b-HCA. In the R of exon 7/8-mutated b-HCA, some little cells are positive for phosphorylated anti-histone 3, whereas hepatocytes are negative. Lack of apoptosis (anti-Casp3) in the adjacent NT tissue in both cases. HES staining is shown for the T, R/OE, and NT areas with the corresponding expression of GS. Positive control for anti-activated Casp3 staining on a section of human amygdala. 5 × magnification, scale bar = 100 μm, insets are zooms on 10 × magnifications. b-HCA, β-catenin-activated HCA; Casp3, caspase 3; GS, glutamine synthetase; HCA, hepatocellular adenoma; HES, H&E saffron; NT, non-tumoural; OE, outer edge; R, tumour rim; T, tumour centre.

was achieved to compare molecular content. Segmentation was via hierarchical clustering; that is, the same spectra are grouped under one colour, meaning similar peptide profiles and thus similar tissue composition. Indeed, mass spectra were clustered into three main classes for exon 3 S45-mutated b-HCA and exon 8/7-mutated b-HCA (Fig. 3A and B). T and R areas display molecular heterogeneity as illustrated by their difference in clustering. MSI analysis from T, R, and NT areas matched perfectly with adjacent tissue section staining (H&E and GS) (A1 to A4 in Fig. 3A and B). The difference in molecular profiles between the three different areas was confirmed by PCA (B1 and B2 in Fig. 3A and B) upon comparison of spectral profiles (C in Fig. 3A and B). These analyses separate the R from both the T and the NT, with the R found at the interface between these two other areas. Deeper analyses of MSI segmentation showed that the spectral profiles of the R were more similar to the profiles of NT areas than to those of T areas (Fig. 3).

We then used LC-MS/MS proteomic profiling to identify and compare the relative abundances of proteins in each ROI previously isolated by laser capture microdissection. We identified an average of 1,268 proteins (identified with at least two specific peptides) from 1 mm^2 of tissue (5-μm-thick section). We considered a variation in expression when the relative abundance ratios were ≥2 or ≤0.5.

First, we compared the ratios between the R and the T between exon 3 S45 and exon 7/8 of b-HCA, and we found no significant differences. To characterise this morphological feature and reveal the proteins differentially expressed in the R, we pooled exon 3 S45 and exon 7/8 of b-HCA subtypes. There were adequate differences among the patterns of deregulation between R and T areas of exon 3 S45-mutated b-HCA and exon 7/8-mutated b-HCA to distinguish expression profiles by PCA (Fig. 4A). Here, 40 proteins were significantly differentially expressed (20 downregulated proteins and 20 upregulated proteins) (Fig. 4B and C). In contrast, only three proteins were significantly differentially expressed between the OE and T of exon 3 non-S45-mutated b-HCA (Fig. 4D).

These data further confirm the observation made by IHC on the tumour heterogeneity between the Rs and Ts of exon 3 S45-mutated b-HCA and exon 7/8-mutated b-HCA. We did not find any significant differences between the proteomic profiles of the tumour OE of exon 3 non-S45-mutated b-HCA and the rest of the tumour (Fig. 4B). Interestingly, there was no difference at the OE of exon 3 non-S45-mutated b-HCA compared with the rest of the tumour (Fig. 4D).

To better understand this difference in phenotype, we explored the biological functions associated with the 40 proteins identified as differentially deregulated in the Rs of exon 3 S45-mutated b-HCA and exon 7/8-mutated b-HCA by gene set enrichment analysis. Our data revealed three major deregulated functions in the Rs: proteins mainly related to amino acid metabolism (including GS), proteins mainly related to lipid metabolism, and proteins that form part of or are associated with collagen matrices (Fig. 5A). We also identified five proteins upregulated in the R that are known targets of the β-catenin pathway (GS[7] R/T = 5.26, OGN[22] R/T = 3.06, ACAA1[23] R/T = 2.23, AMACR[24] R/T = 2.56, and cytochrome P4501A2 [CYP1A2][25] R/T = 2.60) (Fig. 5B).

We noticed, with the exception of proteins involved in fatty acid degradation, that the proteins found expressed in the R *vs.* the T varied in the same way as protein expression varies in the context of normal liver zonation, that is, perivenous hepatocyte *vs.* periportal hepatocyte protein expression (Fig. 5B). For example, CYP1A2 is exclusively expressed in the cytoplasm of perivenous hepatocytes and regulates oxidative stress in the normal liver. A functional link between CYP1A2 and the Wnt/β-catenin pathway has been shown in β-catenin knockout mice and in human hepatocytes.[25,26] We thus analysed the expression profile of CYP1A2 by IHC. We found a perivenous expression of CYP1A2 in NT areas, as expected, a slight expression in the T, but

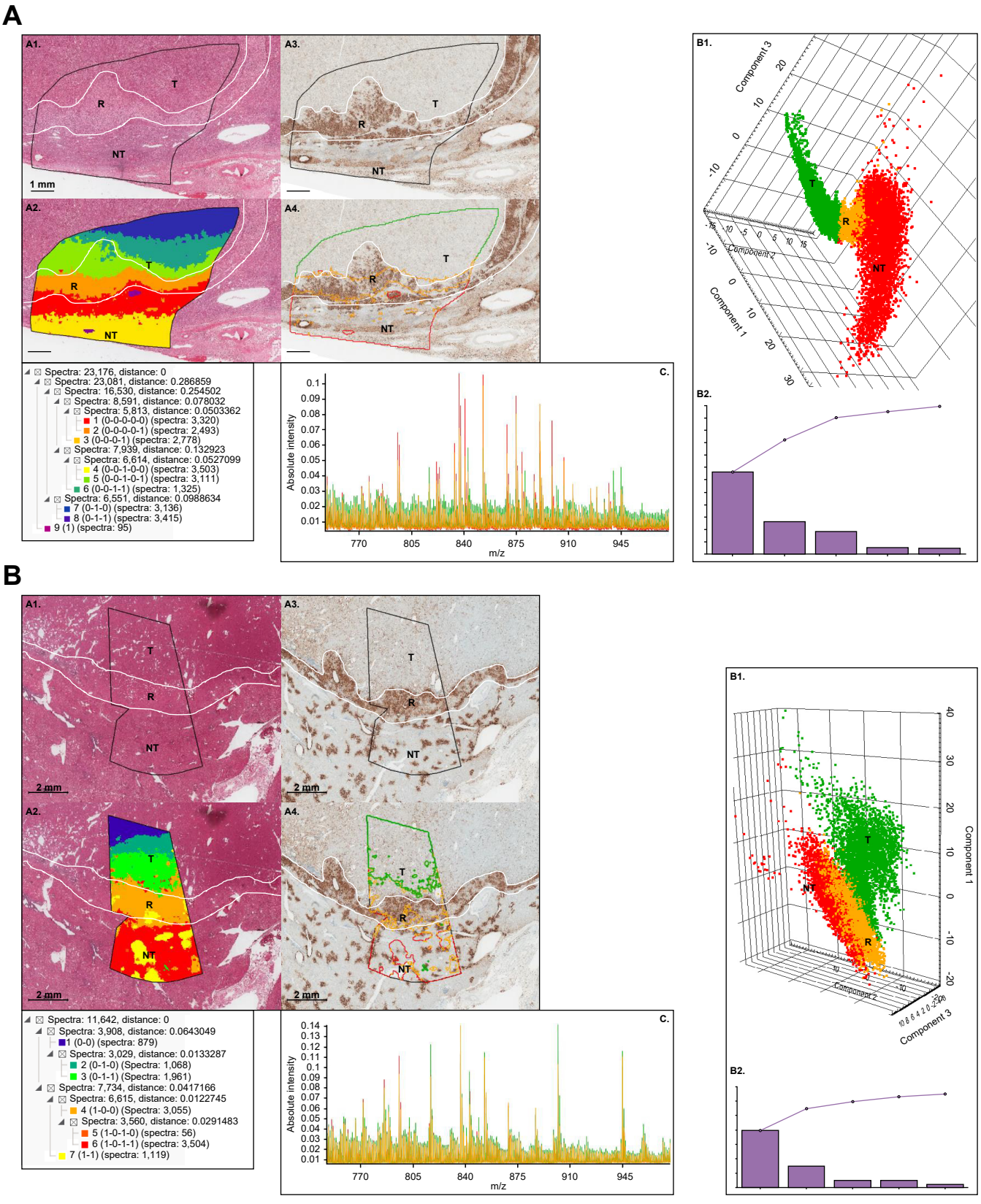

Fig. 3. MSI analysis of exon 7/8-mutated b-HCA and exon 3 S45-mutated b-HCA. (A) Multi-imaging analysis of b-HCA. (A1 and A3) T, R, and NT areas selected (white line boundaries) on successive HES- and GS-stained sections compared with the MSI acquisition area (black). (A2) Clustering analysis by pipeline segmentation using SCiLS Lab Pro 2023a software to overlay HES staining with T, R, and NT annotations. (A4) Corresponding MSI segmentation annotations (red to blue = T, orange = R, and yellow and red = NT) overlaid with GS staining. (B1) Three-dimensional principal component analysis based on the T (green), R (orange), and NT (red) areas obtained from MSI segmentation with explained variance (B2). (C) Mean mass spectra overlay of the T (green), R (orange), and NT (red) areas from a 770 to 945 *m/z* peptide mass range. b-HCA, β-catenin-activated HCA; GS, glutamine synthetase; HCA, hepatocellular adenoma; HES, H&E saffron; MSI, mass spectrometry imaging; NT, non-tumoural; R, tumour rim; T, tumour centre.

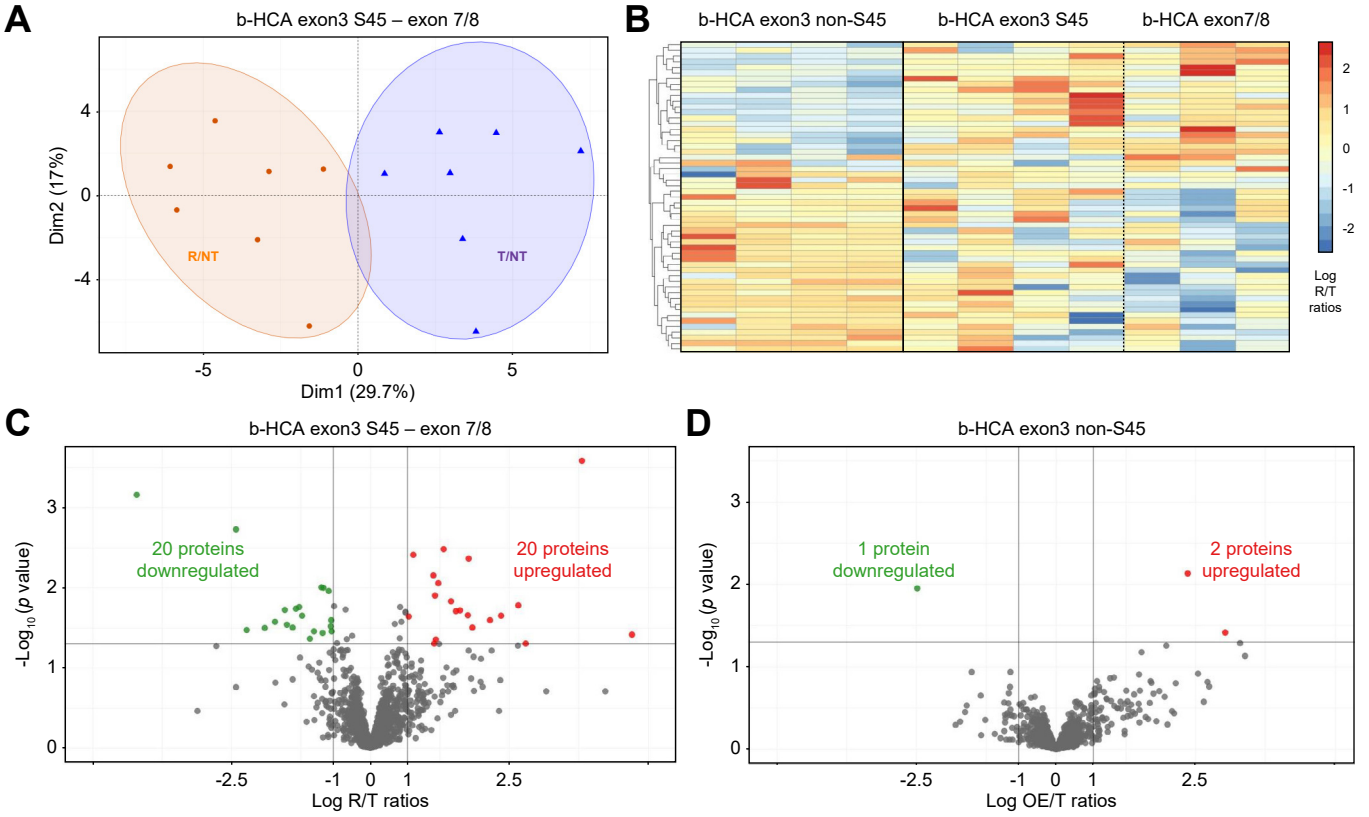

Fig. 4. Proteomic profiling of b-HCA. T, R, and NT areas were isolated by laser capture microdissection, and proteins were extracted for analysis by LC-MS/MS. (A) Principal component analysis comparing the R/T (orange) and T/NT (blue) ratios of exon 3 S45-mutated b-HCA and exon 7/8-mutated b-HCA. (B) Heatmap of the 40 differentially expressed proteins between R and T areas of exon 3 S45-mutated b-HCA (four cases) and exon 7/8-mutated b-HCA (three cases) compared with OE/T ratios of exon 3 non S45-mutated b-HCA (left). (C and D) Volcano plots showing the difference in expression of proteins identified and quantified by proteomic analysis between (C) R and T areas in exon 3 S45-mutated b-HCA and exon 7/8-mutated b-HCA (among the 1,268 proteins identified with at least two specific peptides, 20 proteins were significantly upregulated [red] and 20 proteins were significantly downregulated [green] in the R relative to the T) and (D) the TF and T of exon 3 non-S45-mutated b-HCA. *p* values were calculated with Mann and Withney *t* test. Only two proteins were significantly upregulated (red) and one protein was significantly downregulated (green) in the TF compared with T. b-HCA, β-catenin-activated HCA; GS, glutamine synthetase; HCA, hepatocellular adenoma; LC-MS/MS, liquid chromatography–tandem mass spectrometry; NT, non-tumoural; OE, outer edge; R, tumour rim; T, tumour centre; TF, tumoural front.

a systematic CYP1A2 overexpression in the R. It is noteworthy that this CYP1A2 expression in the R overlaid with GS expression (Fig. 5C). Similarly, AMACR, a crucial enzyme for the β-oxidation of fatty acids and the synthesis of bile acids,[27] is a known target of β-catenin, whose expression level may vary in the event of mutation of the *CTNNB1* gene in HCC.[24] We confirmed by IHC that this protein, which has a perivenous expression profile in the NT liver, is clearly overexpressed in the Rs of exon 3 S45-mutated b-HCA and exon 7/8-mutated b-HCA (Fig. 5C).

Finally, we hypothesised that the overexpression of perivenous proteins in the R could be caused by functional peripheral venous drainage. We confirmed it by analysing the expression profile of stabilin-2, highly expressed on normal human liver sinusoidal endothelial cells (LSECs).[28] Stabilin-2 expression in the tumour is strictly limited to the R, where CD34, a marker of capillarised sinusoids, is negative, whereas CD34 is expressed in the rest of the tumour (Fig. 5D).

Discussion

Consistent with this R overexpressing GS,[16] we showed intratumoural protein expression heterogeneity in exon 3 S45-mutated b-HCA and exon 7/8-mutated b-HCA, contrary to exon 3 non-S45-mutated b-HCA, using MSI and LC-MS/MS approaches. Indeed, we identified different protein expression profiles for the R in comparison with the rest of tumour despite identical β-catenin mutations. Overall, we show that an area with stronger GS expression specifically in the R by IHC can be used for the diagnosis of exon 3 S45-mutated b-HCA or exon 7/8-mutated b-HCA subtypes.[16]

Our former study showed that this R is indeed part of the same tumour by showing C-reactive protein positivity in b-IHCA.[16] In this study, we provided additional evidence by identifying the same β-catenin mutation by DNA sequencing of the R compared with the T. We did not find any significant differences in hepatocyte density or the percentage of proliferative cells in the T *vs*. the R, or in the number of apoptotic cells in the adjacent NT area to the R, thus in all suggesting that the R is not a tumour progression front. In addition, the proteomic profile of this R does not overlap with the proteomic profile of HCA undergoing malignant transformation. An overlap in profiles would require not only a second mutational hit[11] but also proliferation within the tumours, despite them being benign.

HCAs have always been considered as clonal tumours.[29] However, a second or multiple mutations in the R could induce differential protein expression.[11] This hypothesis cannot be

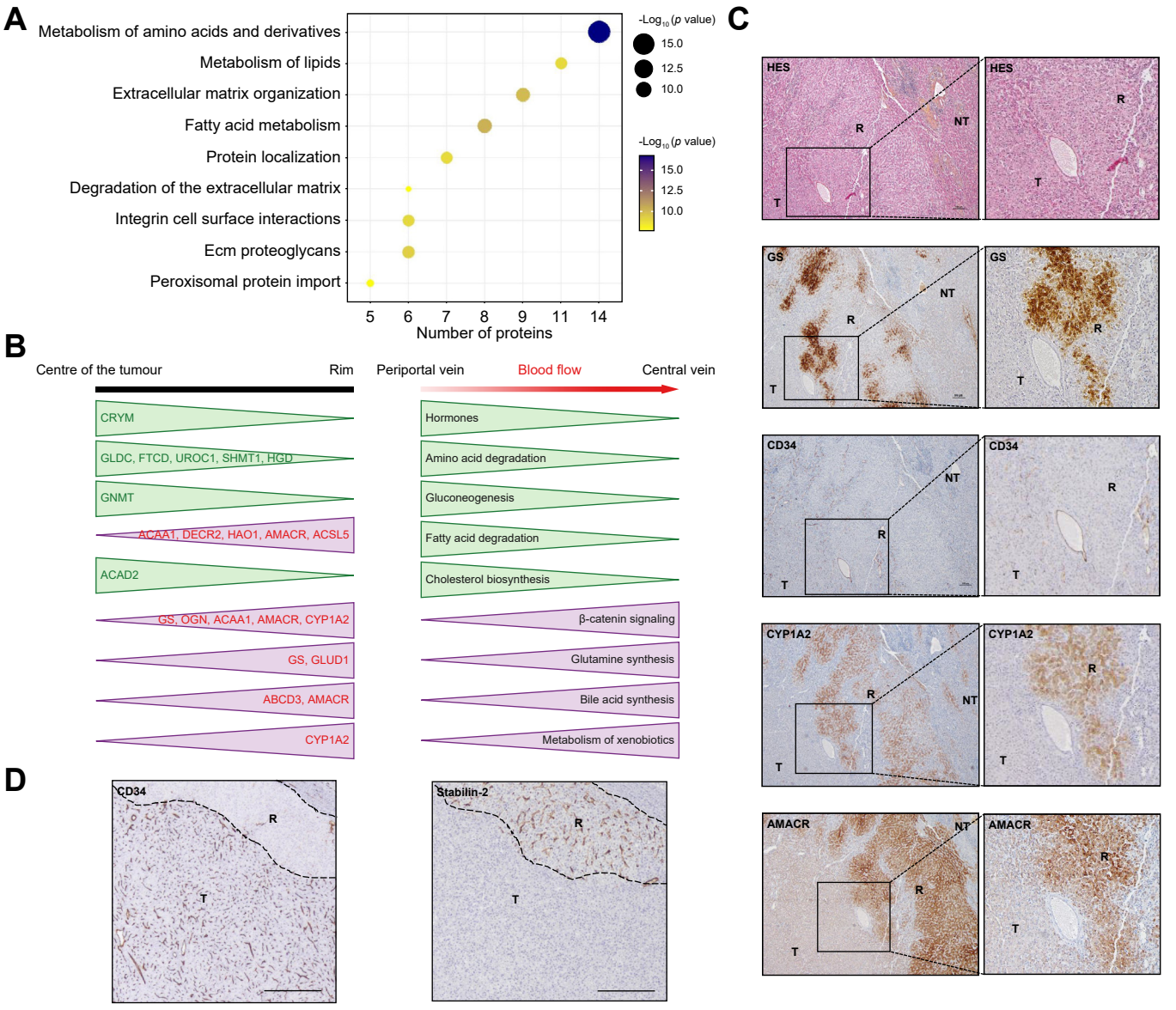

Fig. 5. Functions of differentially expressed proteins in tumor rim. (A) Gene set-enrichment analysis of the 40 differentially expressed proteins between R and T areas of exon 3 S45-mutated b-HCA and exon 7/8-mutated b-HCA performed against the Reactome database. (B) Schematic comparison of the differences in protein expression between R and T areas of exon 3 S45-mutated b-HCA and exon 7/8-mutated b-HCA (left) and the separation of biological pathways between the perivenous and periportal zones in a context of normal liver zonation (right). (C) Immunohistochemical analysis of CYP1A2 and AMACR expression (in comparison with GS expression) in the R of an exon 7/8-mutated b-HCA. HES, anti-GS, and anti-CD34 stainings are shown on serial sections. The boundary between the T, R, and NT areas is highlighted by dotted lines. 5 × magnification, scale bar = 100 μm, insets are zooms on 10 × magnifications. (D) Inverse expression of stabilin-2 (normal positive expression in the R and no expression in the T) and CD34 (positivity in the T contrary to that in the R) in an exon 7/8-mutated b-HCA. Scale bar = 500 μm. Fig. 5B was created using BioRender. b-HCA, β-catenin-activated HCA; CYP1A2, cytochrome P4501A2; GS, glutamine synthetase; HCA, hepatocellular adenoma; HES, H&E saffron; NT, non-tumoural; R, tumour rim; T, tumour centre.

excluded and remains to be verified by whole exome sequencing after laser capture microdissection and separation of these two tissue areas. Another hypothesis concerns the influence of the microenvironment that can also modify protein expression of tumoural hepatocytes. This former hypothesis is more in line with the difference in vascularisation previously illustrated by CD34 negativity in the R as opposed to the diffuse labelling in the T.[17] This observation is unique in the field of benign HCA pathology and has already been reported in a few investigations[16,30] and pathology textbooks.[31] Another feature that deserves attention is the presence of abnormal vessels,[30] possibly dilated sinusoids, generally found close to the R.

We speculate that the mechanism leading to GS expression in the R could be close to the GS expression pattern around hepatic veins in the peripheral tumoural liver despite the fact that Rs are irregular in width and density.

CD34 and stabilin-2 are mutually exclusive markers of LSECs in the normal liver. These LSECs play several major functions in hepatic homoeostasis (sieve, scavenger, and immune) and play a role in regulation of liver microcirculation and metabolism.[28] The

combination of a diffuse CD34 staining in the T (with the presence of abnormal vessels) and a $GS^+/CD34^-$ R leads us to put forward the theory of an abnormal blood flow drainage in the T as opposed to a normal blood flow drainage in the R. In addition, the observation of a normal expression of stabilin-2 in the sinusoidal endothelial cells of the R is a strong argument in favour of this normal R vascularisation.

Moreover, among the 40 proteins shown to be significantly differentially expressed between the T and the R, almost half are found expressed in perivenous zones in a normal hepatocyte context. This is consistent with the clustering of the spectral profiles of the R and adjacent NT areas revealed by MSI.

In addition, it is known that the expression of GS is also regulated by external factors, such as nutrients, drugs, or hormonal factors.[32] This is also the case for CYP1A2 and AMACR, identified in this study with a GS-like expression profile. It is possible that the extensive venous drainage observed at the R contributes to the maintenance of normal hepatocyte functions. IHC results of CYP1A2 and AMACR on both exon 3 S45-mutated and exon 7/8-mutated b-HCA were consistent with proteomic results validating that the extensive venous drainage applies to both subtypes.

In comparison with b-IHCA, exon 3 S45-mutated b-HCA and exon 7/8-mutated b-HCA are more prone to bleeding.[4,6] Interestingly enough, morphological vascular abnormalities are less marked and inconstant in b-IHCA than in b-HCA. The functional effects of this R on tumoural physiopathology remain to be investigated.

This heterogeneity in protein expression means that many factors can regulate gene expression beyond the causative mutation and can therefore contribute to different clinicopathological phenotypes. Here, GS overexpression in the R occurs in a different context to that of β-catenin pathway activation responsible for promoting HCC transformation in exon 3 non-S45-mutated b-HCA. Moreover, our proteomic profile of Rs from exon 3 S45-mutated b-HCA and exon 7/8-mutated b-HCA is distinct to the proteomic profile of HCAs transformed into HCC, which correlates with the finding of a low risk of transformation of exon 3 S45-mutated b-HCA and exon 7/8-mutated b-HCA.

In conclusion, using several advanced and complementary spatial approaches (MSI or the combination of laser capture microdissection with genetic analysis or LC/MS-MS proteomic profiling on FFPE tissue), we were able to analyse tumour heterogeneity of the b-HCA subtype and provide elements of biological interpretation. Next, the culture of human HCA-derived cells will provide new opportunities and the creation of *in vivo* models will contribute to the functional characterisation of the biological pathways involved in the pathophysiology of HCA development. In perspective, transposing a spatial approach to explore tumour heterogeneity in HCC or the tumour immune microenvironment deems useful and could allow for a better understanding of the complexity of liver tumours as well as being a major step in the identification of new and specific targets.

Abbreviations

b-HCA, β-catenin-activated HCA; b-IHCA, β-catenin-activated IHCA; CYP1A2, cytochrome P4501A2; FFPE, formalin-fixed, paraffin-embedded; GS, glutamine synthetase; HCA, hepatocellular adenoma; HCC, hepatocellular carcinoma; IHC, immunohistochemistry; HES, H&E saffron; IHCA, inflammatory HCA; LC-MS/MS, liquid chromatography–tandem mass spectrometry; LSEC, liver sinusoidal endothelial cell; MALDI, matrix-assisted laser desorption/ionisation; MS, mass spectrometry; MSI, mass spectrometry imaging; NT, non-tumour; OE, outer edge; PCA, principal component analysis; ROI, region of interest; R, tumour rim; T, tumour centre; TF, tumoural front; TOF, time of flight.

Financial support

This work was supported by the Nouvelle Aquitaine Region (European FEDER Funds), the Aquitaine Science Transfert, and the SIRIC BRIO. SDT, CD, and AAR were supported by the Nouvelle Aquitaine Region (European FEDER Funds) and the HepA association.

Conflicts of interest

The authors declare that they have no conflicts of interest.

Please refer to the accompanying ICMJE disclosure forms for further details.

Authors' contributions

Laser capture microdissection and sample preparation for LC-MS/MS analysis: SDT. Bioinformatic and biostatistic processing of proteomic data, and graphical data representation: CD. Sample preparation, LC-MS/MS analysis, and data processing: JWD. Immunohistochemistry, imaging, and image analysis: NDS. Genetic sequencing: DC. MALDI imaging and data interpretation: HC, VP. Patient selection: JFB, BLB, CB, PBS. Selection of tissue areas: PBS, VP. LC-MS/MS data processing, integrative biology, and proteomic data interpretation: AAR. Study design: AAR, FS, PBS, CB. Drafting of the manuscript: AAR, FS, PBS, CB, VP.

Data availability statement

The data supporting the results of this study can be found in this article. In addition, the mass spectrometry proteomic data are available through the ProteomeXchange Consortium via the PRIDE partner repository with dataset ID PXD031323. All the reagents, antibodies and resources used in this research are listed in the CTAT table.

Supplementary data

Supplementary data to this article can be found online at https://doi.org/10.1016/j.jhepr.2023.100913.

References

Author names in bold designate shared co-first authorship

[1] Edmondson HA, Henderson B, Benton B. Liver-cell adenomas associated with use of oral contraceptives. N Engl J Med 1976;294:470–472.
[2] Nault J-C, Bioulac-Sage P, Zucman-Rossi J. Hepatocellular benign tumors – from molecular classification to personalized clinical care. Gastroenterology 2013;144:888–902.
[3] Van Aalten SM, de Man RA, Ijzermans JNM, Terkivatan T. Systematic review of haemorrhage and rupture of hepatocellular adenomas. Br J Surg 2012;99:911–916.
[4] Julien C, Le-Bail B, Ouazzani Touhami K, Frulio N, Blanc J-F, Adam J-P, et al. Hepatocellular adenoma risk factors of hemorrhage: size is not the only concern!: single-center retrospective experience of 261 patients. Ann Surg 2021;274:843–850.
[5] Stoot JHMB, Coelen RJS, De Jong MC, Dejong CHC. Malignant transformation of hepatocellular adenomas into hepatocellular carcinomas: a systematic review including more than 1600 adenoma cases. HPB (Oxford) 2010;12:509–522.
[6] Nault J-C, Couchy G, Balabaud C, Morcrette G, Caruso S, Blanc J-F, et al. Molecular classification of hepatocellular adenoma associates with risk

factors, bleeding, and malignant transformation. Gastroenterology 2017;152:880–894.e6.
[7] Bioulac-Sage P, Rebouissou S, Thomas C, Blanc J-F, Saric J, Sa Cunha A, et al. Hepatocellular adenoma subtype classification using molecular markers and immunohistochemistry. Hepatology 2007;46:740–748.
[8] Zucman-Rossi J, Villanueva A, Nault J-C, Llovet JM. Genetic landscape and biomarkers of hepatocellular carcinoma. Gastroenterology 2015;149:1226–1239.e4.
[9] **Dourthe C**, **Julien C**, Di Tommaso S, Dupuy J-W, Dugot-Senant N, Brochard A, et al. Proteomic profiling of hepatocellular adenomas paves the way to diagnostic and prognostic approaches. Hepatology 2021;74:1595–1610.
[10] Bayard Q, Caruso S, Couchy G, Rebouissou S, Bioulac-Sage P, Balabaud C, et al. Recurrent chromosomal rearrangements of *ROS1, FRK* and *IL6* activating JAK/STAT pathway in inflammatory hepatocellular adenomas. Gut 2020;69:1667–1676.
[11] Rebouissou S, Franconi A, Calderaro J, Letouzé E, Imbeaud S, Pilati C, et al. Genotype-phenotype correlation of CTNNB1 mutations reveals different ß-catenin activity associated with liver tumor progression. Hepatology 2016;64:2047–2061.
[12] Nault JC, Mallet M, Pilati C, Calderaro J, Bioulac-Sage P, Laurent C, et al. High frequency of telomerase reverse-transcriptase promoter somatic mutations in hepatocellular carcinoma and preneoplastic lesions. Nat Commun 2013;4:2218.
[13] **Henriet E**, **Abou Hammoud A**, Dupuy J-W, Dartigues B, Ezzoukry Z, Dugot-Senant N, et al. Argininosuccinate synthase 1 (ASS1): a marker of unclassified hepatocellular adenoma and high bleeding risk. Hepatology 2017;66:2016–2028.
[14] Sala M, Gonzales D, Leste-Lasserre T, Dugot-Senant N, Paradis V, Di Tommaso S, et al. ASS1 Overexpression: a hallmark of sonic hedgehog hepatocellular adenomas; recommendations for clinical practice. Hepatol Commun 2020;4:809–824.
[15] Thomeer MG, Broker M, Verheij J, Doukas M, Terkivatan T, Bijdevaate D, et al. Hepatocellular adenoma: when and how to treat? Update of current evidence. Therap Adv Gastroenterol 2016;9:898–912.
[16] Sempoux C, Gouw ASH, Dunet V, Paradis V, Balabaud C, Bioulac-Sage P. Predictive patterns of glutamine synthetase immunohistochemical staining in CTNNB1-mutated hepatocellular adenomas. Am J Surg Pathol 2021;45:477–487.
[17] Sempoux C, Balabaud C, Bioulac-Sage P. Malignant transformation of hepatocellular adenoma. Hepat Oncol 2014;1:421–431.
[18] Bioulac-Sage P, Sempoux C, Balabaud C. Hepatocellular adenoma: classification, variants and clinical relevance. Semin Diagn Pathol 2017;34:112–125.
[19] Bouyssié D, Hesse A-M, Mouton-Barbosa E, Rompais M, Macron C, Carapito C, et al. Proline: an efficient and user-friendly software suite for large-scale proteomics. Bioinformatics 2020;36:3148–3155.
[20] Perez-Riverol Y, Csordas A, Bai J, Bernal-Llinares M, Hewapathirana S, Kundu DJ, et al. The PRIDE database and related tools and resources in 2019: improving support for quantification data. Nucleic Acids Res 2019;47:D442–D450.
[21] Levayer R. Solid stress, competition for space and cancer: the opposing roles of mechanical cell competition in tumour initiation and growth. Semin Cancer Biol 2020;63:69–80.
[22] Du L, Qian X, Dai C, Wang L, Huang D, Wang S, et al. Screening the molecular targets of ovarian cancer based on bioinformatics analysis. Tumori 2015;101:384–389.
[23] Frey JL, Kim SP, Li Z, Wolfgang MJ, Riddle RC. β-Catenin directs long-chain fatty acid catabolism in the osteoblasts of male mice. Endocrinology 2018;159:272–284.
[24] Sekine S, Ogawa R, Ojima H, Kanai Y. Overexpression of α-methylacyl-CoA racemase is associated with CTNNB1 mutations in hepatocellular carcinomas. Histopathology 2011;58:712–719.
[25] Tan X, Behari J, Cieply B, Michalopoulos GK, Monga SPS. Conditional deletion of beta-catenin reveals its role in liver growth and regeneration. Gastroenterology 2006;131:1561–1572.
[26] Gerbal-Chaloin S, Dumé A-S, Briolotti P, Klieber S, Raulet E, Duret C, et al. The WNT/β-catenin pathway is a transcriptional regulator of *CYP2E1, CYP1A2*, and aryl hydrocarbon receptor gene expression in primary human hepatocytes. Mol Pharmacol 2014;86:624–634.
[27] Lloyd MD, Darley DJ, Wierzbicki AS, Threadgill MD. α-Methylacyl-CoA racemase – an 'obscure' metabolic enzyme takes centre stage: α-Methylacyl-CoA racemase and cancer. FEBS J 2008;275:1089–1102.
[28] Sørensen KK, Simon-Santamaria J, McCuskey RS, Smedsrød B. Liver sinusoidal endothelial cells. Compr Physiol 2015;5:1751–1774.
[29] Castelli G, Pelosi E, Testa U. Liver cancer: molecular characterization, clonal evolution and cancer stem cells. Cancers (Basel) 2017;9:127.
[30] Bioulac-Sage P, Gouw ASH, Balabaud C, Sempoux C. Hepatocellular adenoma: what we know, what we do not know, and why it matters. Histopathology 2022;80:878–897.
[31] Bioulac-Sage P. WHO classification of tumors. 5th ed. Switzerland: World Health Organization (WHO) International agency for research on cancer; 2019.
[32] Gebhardt R, Baldysiak-Figiel A, Krügel V, Ueberham E, Gaunitz F. Hepatocellular expression of glutamine synthetase: an indicator of morphogen actions as master regulators of zonation in adult liver. Prog Histochem Cytochem 2007;41:201–266.